

Recursive T matrix algorithm for resonant multiple scattering : Applications to localized plasmon excitations

Brian Stout¹ and J.C. Auger² and Alexis Devilez¹

¹*Case 161, Institut Fresnel, Faculté des Sciences et Techniques de St. Jérôme
13397 Marseille cedex 20, France*

²*Center for Laser Diagnostics, Dept. of Applied Physics and
Yale University, New Haven, CT 06520 USA**

(Dated: July 2008)

A matrix balanced version of the Recursive Centered T Matrix Algorithm (RCTMA) applicable to systems possessing *resonant* inter-particle couplings is presented. Possible domains of application include systems containing interacting localized plasmon resonances, surface resonances, and photonic jet phenomena. This method is of particular interest when considering modifications to complex systems. The numerical accuracy of this technique is demonstrated in a study of particles with strongly interacting localized plasmon resonances.

© 2018 Optical Society of America

OCIS codes:

Keywords: Multiple scattering, T matrices, morphology dependent resonances, plasmon resonances

1. Introduction

It has been well established that certain kinds of recursive T matrix algorithms (known as RCTMA)^{1,2} are numerically stable and can be used to solve the Foldy-Lax multiple-scattering equations for particles exhibiting “modest” inter-particle couplings. By “modest couplings”, we refer to situations in which the order of orbital number of the Vector Spherical

*Electronic address: brian.stout@fresnel.fr, augerjc@gmail.com, alexis.devilez@fresnel.fr

Wave Functions (VSWFs) necessary to describe the field scattered by each particle in an aggregate of particles are not too much larger than that necessary for describing isolated particles. The “modest coupling” criteria apply to a host of multiple scattering situations, including systems of dielectric particles comparable in size to the wavelength and for most packing fractions including dense packing. The modest coupling criteria can also apply to metallic particles under certain conditions.

Like any multiple scattering technique not employing matrix balancing, the RCTMA can encounter numerical difficulties in certain extreme situations of strongly coupled resonant phenomenon. In this work, we present a matrix balanced form of the Recursive Centered T Matrix Algorithm (or RCTMA) that can readily be employed even in the presence of strong (*i.e.* resonant) inter-particle couplings. The rather extreme situation of “strong couplings” studied here will generally require carefully micro-scaled engineered systems where high Q -factor resonances can occur for particles illuminated in isolation, and in which the particles are sufficiently closely spaced that neighboring particles modify the resonance response properties. Examples of strong inter-particle couplings can be found in particles exhibiting plasmon resonances, surface resonances, or even photonic jet phenomenon.

In section 2, the notation is introduced in a brief review of the relevant multiple-scattering theory. Section 3 describes an analytic matrix balancing procedure used to ‘well-condition’ the multiple scattering system of equations. A matrix balanced RCTMA is derived in section 4. Essential formulas for applications are summarized in section 5. Their applications are then demonstrated by applying matrix balanced RCTMA calculations to study systems of interacting localized plasmon excitations. Some known and novel aspects of interacting localized plasmon excitations are presented herein.

2. Multiple-scattering theory - VSWF approach

Let us consider an arbitrary incident electromagnetic field incident on a collection of three-dimensional particles (as shown in fig.1). The particles are considered as ‘individual’ scatterers if they can be placed in a circumscribing sphere lying entirely within the homogeneous medium (actually this constraint can frequently be relaxed, cf.³).

The electromagnetic field incident on an N -particle system, \mathbf{E}_i , is developed in terms of the transverse *regular* VSWFs developed about some point \mathbf{O} arbitrarily chosen as the

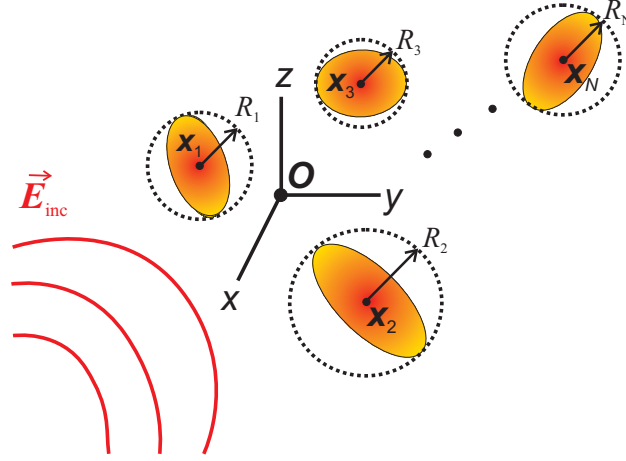


Fig. 1. Schematic of an field incident on a collection of scatterers centered on $\mathbf{x}_1, \mathbf{x}_2, \dots, \mathbf{x}_N$. The radii of the respective circumscribing spheres are denoted R_1, R_2, \dots, R_N .

system ‘origin’:

$$\begin{aligned} \mathbf{E}_i(\mathbf{r}) &= E_0 \sum_{n=1}^{\infty} \sum_{m=-n}^n \{ Rg[\mathbf{M}_{nm}(k\mathbf{r})] a_{1,n,m} + Rg[\mathbf{N}_{nm}(k\mathbf{r})] a_{2,n,m} \} \\ &= E_0 \sum_{q=1}^2 \sum_{p=1}^{\infty} Rg[\Psi_{q,p}(k\mathbf{r})] a_{q,p} \equiv E_0 Rg[\Psi^t(k\mathbf{r})] a \end{aligned} \quad (1)$$

where E_0 is a real parameter determining the incident field amplitude. Eq.(1), introduces a condensed notation for the VSWFs, \mathbf{M}_{nm} and \mathbf{N}_{nm} : $\Psi_{1,p}(k\mathbf{r}) \equiv \mathbf{M}_{n,m}(k\mathbf{r})$ and $\Psi_{2,p}(k\mathbf{r}) \equiv \mathbf{N}_{n,m}(k\mathbf{r})$. The notation $Rg[\]$ stands for “the regular part of” and distinguishes these regular VSWFs from the “irregular” scattered VSWFs (cf. appendix A). In the second line of eq.(1), the two subscripts (n, m) are replaced by a single subscript p defined such that $p(n, m) \equiv n(n+1) - m$ and has the inverse relations⁴:

$$n(p) = \text{Int}\sqrt{p} \quad m(p) = -p + n(n+1) . \quad (2)$$

The last line of eq.(1), adopts the compact matrix notation allowing the suppression of the summation symbols.⁵ The superscripted $(^t)$ stands for the transpose of a column ‘matrix’ of composed of VSWFs into a row ‘matrix’ of these functions.

For points external to all individual circumscribing spheres, the total field, $\mathbf{E}_t(\mathbf{r})$ can be written as the sum of the incident field, and a set of ‘individual’ scattered fields, $\mathbf{E}_s^{(j)}$,

centered respectively on each of the particle centers:

$$\begin{aligned}\mathbf{E}_t(\mathbf{r}) &= \mathbf{E}_i(\mathbf{r}) + \sum_{j=1}^N \mathbf{E}_s^{(j)}(\mathbf{r}_j) \\ &= E_0 \text{Rg}[\Psi^t(k\mathbf{r})] a + E_0 \sum_{j=1}^N \Psi^t(k\mathbf{r}_j) f_N^{(j)}\end{aligned}\quad (3)$$

where each scattered field, $\mathbf{E}_s^{(j)}$, is developed, with coefficients $f_N^{(j)}$, on a basis of outgoing VSWFs defined with respect to the associated particle center, denoted \mathbf{x}_j . The spherical coordinates relative to each scatterer are denoted $\mathbf{r}_j \equiv \mathbf{r} - \mathbf{x}_j$.

The crucial idea of Foldy-Lax multiple-scattering theory is that there exists an excitation field, $\mathbf{E}_{\text{exc}}^{(j)}(\mathbf{r})$, associated with each particle which is the superposition of the incident field and the field scattered by all the other particles in the system (excluding the field scattered by the particle itself).⁶ From this definition, the excitation field of the j^{th} particle can be written

$$\begin{aligned}\mathbf{E}_{\text{exc}}^{(j)}(\mathbf{r}_j) &\equiv E_0 \text{Rg}[\Psi^t(k\mathbf{r}_j)] e_N^{(j)} \equiv \mathbf{E}_i(\mathbf{r}) + \sum_{l=1, l \neq j}^N \mathbf{E}_s^{(l)}(\mathbf{r}_l) \\ &= E_0 \text{Rg}[\Psi^t(k\mathbf{r}_j)] \left[J^{(j,0)} a + \sum_{l=1, l \neq j}^N H^{(j,l)} f_N^{(l)} \right]\end{aligned}\quad (4)$$

where $e_N^{(j)}$ are the coefficients of the excitation field in a regular VSWF basis centered on the j^{th} particle. In the second line of eq.(4), we have used the translation-addition theorem^{1,4,5}) and introduced the notation where $J^{(j,0)} \equiv J(k\mathbf{x}_j)$ is a regular translation matrix and $H^{(j,l)} \equiv H[k(\mathbf{x}_j - \mathbf{x}_l)]$ is an irregular translation matrix. Analytical expressions for the matrix elements of $J(k\mathbf{x}_j)$ and $H(k\mathbf{x}_j)$ are given in refs.^{1,4}.

The other key idea of multiple scattering theory is that the field scattered by the object, $f_N^{(j)}$, is obtained from the excitation field $e_N^{(j)}$ via the 1-body T matrix, $T_1^{(j)}$, derived when one considers the particle to be immersed in an infinite homogeneous medium. This relation is then expressed as

$$f_N^{(j)} = T_1^{(j)} e_N^{(j)} \quad (5)$$

[The index 1 on the $T_1^{(j)}$ indicates that this T matrix concerns an isolated particle, henceforth referred to as a ‘1-body’ T matrix.] Employing eq.(5) in eq.(4), one obtains a Foldy-Lax set

of equations for the excitation field coefficients^{1,5}:

$$e_N^{(j)} = J^{(j,0)} a + \sum_{l=1, l \neq j}^N H^{(j,l)} T_1^{(l)} e_N^{(l)} \quad j = 1, \dots, N \quad (6)$$

For numerical applications where one is obliged to solve the equations on a truncated VSWF basis, it is advantageous to work with a set of formally equivalent equations involving the scattering coefficients $f_N^{(j)}$. This set of equations is derived by multiplying each of eqs.(6) from the left by $T_1^{(j)}$ and using eq.(5) to obtain

$$f_N^{(j)} = T_1^{(j)} J^{(j,0)} a + T_1^{(j)} \sum_{l=1, l \neq j}^N H^{(j,l)} f_N^{(l)} \quad j = 1, \dots, N \quad (7)$$

In the RCTMA, one calculates the *centered* multiple scattering transition matrices, $T_N^{(j,k)}$, which directly yield the scattered field coefficients in terms of the field incident on the system through the expression

$$f_N^{(j)} = \sum_{k=1}^N T_N^{(j,k)} a^{(k)} \quad \text{with} \quad a^{(k)} \equiv J^{(k,0)} a \quad (8)$$

In this equation, we have introduced the column matrix $a^{(j)}$ which contains the coefficients of the field incident on the entire system developed on a VSWF basis centered on the j^{th} particle.

3. Basis set truncation and matrix balancing

Although the multiple scattering formulas of the previous section are expressed as matrix equations on VSWF basis sets of infinite dimension, the finite size of the scatterers naturally restricts the dimension of the dominate VSWF contributions. In order to discuss this phenomenon analytically, we consider the case of spherical scatterers. For non-spherical scatterers, the matrix balancing procedure described below should be applied to the circumscribing spheres of the particles.

The Mie solution for a sphere of radius R_j immersed in a homogeneous host medium, can be cast in the form of a 1-body T matrix that is diagonal in a VSWF basis centered on the particle:

$$\left[T_1^{(j)} \right]_{q,p;q',p'} = \delta_{q,q'} \delta_{p,p'} T_1(j, n(p), q) \quad (9)$$

where the $T_1^{(j)}(n(p), q)$ correspond to the Mie coefficients and depend on q and n (cf. eq.(1)).

With the objective of matrix balancing, it is helpful to express the Mie coefficients of the scatterers in terms of the Ricatti Bessel and Hankel functions, respectively $\psi_n(z) \equiv zj_n(z)$ and $\xi_n(z) \equiv zh_n(z)$, and their logarithmic derivatives

$$\Phi_n(z) \equiv \frac{\psi'_n(z)}{\psi_n(z)} \quad \Psi_n(z) \equiv \frac{\xi'_n(z)}{\xi_n(z)} \quad (10)$$

The T matrix elements of eq.(9) for a sphere of dielectric contrast $\rho_j \equiv k_j/k$ can then be cast in the convenient form⁷:

$$\begin{aligned} T(j, n, 1) &= \frac{\psi_n(kR_j)}{\xi_n(kR_j)} \frac{\frac{\mu_j}{\mu} \Phi_n(kR_j) - \rho_j \Phi_n(\rho_j kR_j)}{\rho_j \Phi_n(\rho_j kR_j) - \frac{\mu_j}{\mu} \Psi_n(kR_j)} \equiv \frac{\psi_n(kR_j)}{\xi_n(kR_j)} \bar{T}(j, n, 1) \\ T(j, n, 2) &= \frac{\psi_n(kR_j)}{\xi_n(kR_j)} \frac{\frac{\mu_j}{\mu} \Phi_n(\rho_j kR_j) - \rho_j \Phi_n(kR_j)}{\rho_j \Psi_n(kR_j) - \frac{\mu_j}{\mu} \Phi_n(\rho_j kR_j)} \equiv \frac{\psi_n(kR_j)}{\xi_n(kR_j)} \bar{T}(j, n, 2) \end{aligned} \quad (11)$$

where k is the wavenumber in the external medium. The normalized T matrix coefficients, $\bar{T}(j, n, q)$, of eq.(MieT) contain a rich resonant structure. The ratios $\psi_n(kR_j)/\xi_n(kR_j)$ on the other hand have an exponentially decreasing behavior for large, $n \gg kR_j$ as is demonstrated in fig.2 for $kR = 10$. One can remark from figure 2 that $|\psi_n(kR)/\xi_n(kR)|$ become quite small beyond $n_{\max} = kR + 3$ and its value at $n = 14$ is $\sim 2 \cdot 10^{-4}$. Although these factors permit an appropriately truncated VSWF basis set to contain essentially all the physical information necessary for accurate calculations, they also tend to produce ill-conditioned linear systems when one is obliged to enlarge the VSWF space far beyond $\approx kR + 3$ in order to account for strong coupling phenomenon.

A solution to the above problem is to ‘balance’ the matrix manipulations in section 4 below by defining “normalized” scattering and incident coefficients:

$$\begin{aligned} [\bar{f}^{(j)}]_{q,p} &\equiv \xi_{n(p)}(kR_j) [f^{(j)}]_{q,p} \\ [\bar{a}^{(j)}]_{q,p} &\equiv \psi_{n(p)}(kR_j) [a^{(j)}]_{q,p} \end{aligned} \quad (12)$$

For notational purposes, it is convenient to define diagonal matrices $[\psi^{(j)}]$ and $[\xi^{(j)}]$ with Ricatti-Bessel functions along their diagonals, namely $[\psi^{(j)}]_{q',p';q,p} \equiv \delta_{q,q'} \delta_{p,p'} \psi_{n(p)}(kR_j)$ and $[\xi^{(j)}]_{q',p';q,p} \equiv \delta_{q,q'} \delta_{p,p'} \xi_{n(p)}(kR_j)$. This notation allows normalized or ‘balanced’ versions of the one-body and many-body T -matrices to be defined respectively as

$$\bar{T}_1^{(j)} \equiv [\xi^{(j)}] T_1^{(j)} [\psi^{(j)}]^{-1} \quad \text{and} \quad \bar{T}_N^{(j,k)} \equiv [\xi^{(j)}] \bar{T}_N^{(j,k)} [\psi^{(k)}]^{-1} \quad (13)$$

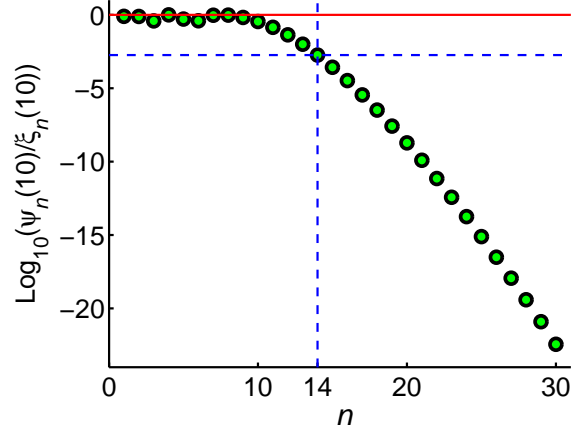


Fig. 2. Plot of the spherical Bessel to Hankel function ratio, $\psi_n(kR)/\xi_n(kR)$ occurring in the Mie coefficients when $kR = 10$.

In terms of these normalized quantities, eq.(8) then reads

$$\bar{f}_N^{(j)} = \sum_{k=1}^N \bar{T}_N^{(j,k)} \bar{a}^{(k)} \quad j = 1, \dots, N \quad (14)$$

In the next section, these ‘normalized’ $\bar{T}_1^{(j)}$ and $\bar{T}_N^{(j,k)}$ are used to derive a matrix balanced version of the recursive T matrix algorithm.

4. Derivation of a matrix balanced recursive algorithm

In this section, we derive a matrix balanced version of the Recursive Centered T Matrix Algorithm (RCTMA) using purely algebraic manipulations. The recursive algorithm can be invoked once we have a solution for the $\bar{T}_{N-1}^{(j,k)}$ matrices of a $N \geq 1$ particle system. If we wish to solely use the recursive algorithm to solve a system, we initiate the recursive process with a single particle solution described by $\bar{T}_1^{(1,1)} \equiv \bar{T}_1^{(1)}$.

One then considers an arbitrarily positioned particle being added to the system. The excitation field on a particle N added to the system can be expressed as the superposition of three fields. The first contribution is simply the field incident on the system, the second contribution results from the scattering of the incident field by the $N - 1$ cluster of particles onto the particle N , and finally the third contribution comes from field scattered by the particle N onto the $N - 1$ cluster and which returns to the N^{th} particle as an excitation field. Invoking the translation-addition theorem and eq.(8), these three contributions can

be expressed in matrix form as¹

$$e_N^{(N)} = a^{(N)} + \sum_{j,k=1}^{N-1} H^{(N,j)} T_{N-1}^{(j,k)} a^{(k)} + \sum_{j,k=1}^{N-1} H^{(N,j)} T_{N-1}^{(j,k)} H^{(k,N)} f_N^{(N)} \quad (15)$$

Defining now the normalized irregular translation matrices and excitation coefficients respectively as

$$\overline{H}^{(j,k)} \equiv [\psi^{(j)}] H^{(j,k)} [\xi^{(k)}]^{-1} \quad \text{and} \quad \overline{e}_N^{(j)} \equiv [\psi^{(j)}] e_N^{(j)} \quad (16)$$

the normalized form of eq.(15) can be written

$$\overline{e}_N^{(N)} = \overline{a}^{(N)} + \sum_{j,k=1}^{N-1} \overline{H}^{(N,j)} \overline{T}_{N-1}^{(j,k)} \overline{a}^{(k)} + \sum_{j,k=1}^{N-1} \overline{H}^{(N,j)} \overline{T}_{N-1}^{(j,k)} \overline{H}^{(k,N)} \overline{f}_N^{(N)} \quad (17)$$

where we also used the definitions in eqs.(12) and (13).

Recalling that the excitation field is linked to the scattered field by the 1-body T -matrix via eq.(5), and invoking the definitions of eq.(12) and (16) we can write

$$\overline{e}_N^{(j)} = \left[\overline{T}_1^{(j)} \right]^{-1} \overline{f}_N^{(j)} \quad (18)$$

Employing this relation for particle N on the LHS of eq.(17) and rearranging we obtain

$$\begin{aligned} & \left\{ \left[\overline{T}_1^{(N)} \right]^{-1} - \sum_{j,k=1}^{N-1} \overline{H}^{(N,j)} \overline{T}_{N-1}^{(j,k)} \overline{H}^{(k,N)} \right\} \overline{f}_N^{(N)} \\ & = \overline{a}^{(N)} + \sum_{j,k=1}^{N-1} \overline{H}^{(N,j)} \overline{T}_{N-1}^{(j,k)} \overline{a}^{(k)}. \end{aligned} \quad (19)$$

We now take the normalized $\overline{T}_N^{(N,N)}$ matrix to be expressed as

$$\overline{T}_N^{(N,N)} = \left\{ \left[\overline{T}_1^{(N)} \right]^{-1} - \sum_{j,k=1}^{N-1} \overline{H}^{(N,j)} \overline{T}_{N-1}^{(j,k)} \overline{H}^{(k,N)} \right\}^{-1} \quad (20)$$

With this assignment, we multiply both sides of eq.(19) by $\overline{T}_N^{(N,N)}$ and obtain an expression consistent with equation (14):

$$\begin{aligned} \overline{f}_N^{(N)} & = \overline{T}_N^{(N,N)} \overline{a}^{(N)} + \overline{T}_N^{(N,N)} \sum_{j,l=1}^{N-1} \overline{H}^{(N,j)} \overline{T}_{N-1}^{(j,k)} \overline{a}^{(k)} \\ & = \overline{T}_N^{(N,N)} \overline{a}^{(N)} + \sum_{l=1}^{N-1} \overline{T}_N^{(N,l)} \overline{a}^{(l)} = \sum_{l=1}^N \overline{T}_N^{(N,l)} \overline{a}^{(l)} \end{aligned} \quad (21)$$

where we have assigned the matrix $\overline{T}_N^{(N,k)}$, $k \neq N$ as

$$\overline{T}_N^{(N,k)} = \overline{T}_N^{(N,N)} \sum_{j=1}^{N-1} \overline{H}^{(N,j)} \overline{T}_{N-1}^{(j,k)} \quad (22)$$

One completes the description of the scattering by the system by remarking that the field scattered by the other particles in the system are the superposition of the field that would be scattered by the $N - 1$ cluster in the absence of the N^{th} particle, plus the field scattered from the $N - 1$ particle originating as a scattered field emanating from the N^{th} particle. Using again the translation-addition theorem, the field coefficients of $\overline{f}_N^{(j)}$ can in turn be expressed in a form consistent with equation (14) as

$$\begin{aligned} \overline{f}_N^{(j)} &= \sum_{l=k}^{N-1} \overline{T}_{N-1}^{(j,k)} \overline{a}^{(k)} + \sum_{k=1}^{N-1} \overline{T}_{N-1}^{(j,k)} \overline{H}^{(k,N)} \overline{f}_N^{(N)} \\ &= \sum_{l=1}^{N-1} \overline{T}_{N-1}^{(j,k)} \overline{a}^{(k)} + \sum_{k=1}^{N-1} \overline{T}_{N-1}^{(j,k)} \overline{H}^{(k,N)} \overline{T}_N^{(N,N)} \overline{a}^{(N)} \\ &\quad + \sum_{l=1}^{N-1} \sum_{k=1}^{N-1} \overline{T}_{N-1}^{(j,l)} \overline{H}^{(l,N)} \overline{T}_N^{(N,k)} \overline{a}^{(k)} \\ &= \overline{T}_N^{(j,N)} \overline{a}^{(N)} + \sum_{k=1}^{N-1} \overline{T}_N^{(j,k)} \overline{a}^{(k)} = \sum_{k=1}^N \overline{T}_N^{(j,k)} \overline{a}^{(k)} \end{aligned} \quad (23)$$

where we invoked eq.(21). In the second and third lines we have defined the $\overline{T}_N^{(j,N)}$ and $\overline{T}_N^{(j,l)}$ matrices such that

$$\overline{T}_N^{(j,N)} = \sum_{k=1}^{N-1} \overline{T}_{N-1}^{(j,k)} \overline{H}^{(k,N)} \overline{T}_N^{(N,N)} \quad (24a)$$

$$\overline{T}_N^{(j,k)} = \overline{T}_{N-1}^{(j,k)} + \sum_{l=1}^{N-1} \overline{T}_{N-1}^{(j,l)} \overline{H}^{(l,N)} \overline{T}_N^{(N,k)} \quad (24b)$$

At this point, all the $\overline{T}_N^{(j,k)}$ matrices have been obtained and the matrix manipulations in eqs.(20), (22) and (24) can then be repeated to add as many particles to the system as desired.

A. Relationship with system matrix inversions

Although the recursive algorithm is quite efficient for systems with relatively small numbers of particles, for systems with many particles, one may prefer to try and solve an entire N -particle system directly. A balanced linear system for the entire system corresponding to

our recursive algorithm can be obtained by applying the relation of eq.(5) to the left hand side of eq.(7), then multiplying both sides of the resulting equations by the $[\psi^{(j)}]$ matrix and finally rearranging to obtain a system of balanced linear equations for the unknown scattering coefficients:

$$\left[\overline{T}_1^{(j)}\right]^{-1} \overline{f}_N^{(j)} - \sum_{k=1, k \neq j}^N \overline{H}^{(j,k)} \overline{f}_N^{(k)} = \overline{a}^{(j)} \quad j = 1, \dots, N \quad (25)$$

where we used eqs.(12) and (13). The system of linear equations in eq.(25) can in principle be directly solved by inverting the balanced system matrix:

$$\begin{bmatrix} \overline{f}_N^{(1)} \\ \overline{f}_N^{(2)} \\ \vdots \\ \overline{f}_N^{(N)} \end{bmatrix} = \begin{bmatrix} \left[\overline{T}_1^{(1)}\right]^{-1} & -\overline{H}^{(1,2)} & \dots & -\overline{H}^{(1,N)} \\ -\overline{H}^{(2,1)} & \left[\overline{T}_1^{(2)}\right]^{-1} & \dots & -\overline{H}^{(2,N)} \\ \vdots & \vdots & \ddots & \vdots \\ -\overline{H}^{(N,1)} & -\overline{H}^{(N,2)} & \dots & \left[\overline{T}_1^{(N)}\right]^{-1} \end{bmatrix}^{-1} \begin{bmatrix} \overline{a}^{(1)} \\ \overline{a}^{(2)} \\ \vdots \\ \overline{a}^{(N)} \end{bmatrix} \quad (26)$$

Once we have inverted this system, one can associate each block with a corresponding $\overline{T}_N^{(j,k)}$ matrix as shown below as

$$\begin{bmatrix} \overline{f}_N^{(1)} \\ \overline{f}_N^{(2)} \\ \vdots \\ \overline{f}_N^{(N)} \end{bmatrix} = \begin{bmatrix} \overline{T}_N^{(1,1)} & \overline{T}_N^{(1,2)} & \dots & \overline{T}_N^{(1,N)} \\ \overline{T}_N^{(2,1)} & \overline{T}_N^{(2,2)} & \dots & \overline{T}_N^{(2,N)} \\ \vdots & \vdots & \ddots & \vdots \\ \overline{T}_N^{(N,1)} & \overline{T}_N^{(N,2)} & \dots & \overline{T}_N^{(N,N)} \end{bmatrix} \begin{bmatrix} \overline{a}^{(1)} \\ \overline{a}^{(2)} \\ \vdots \\ \overline{a}^{(N)} \end{bmatrix} \quad (27)$$

which is the same form as the desired solutions given in eq.(14).

5. Summary and applications to localized plasmon excitations

In this section, we will apply the RCTMA to solve systems exhibiting strong interactions between localized plasma resonances. We begin this section by summarizing the balanced recursive algorithm. We then recall some useful formulas for extracting physical quantities from the T matrix. Finally, we carry out some illustrative calculations for strongly interacting systems.

A. Summary of the balanced RCTMA algorithm

In order to implement the RCTMA, one must first solve the 1-body T -matrices, $T_1^{(1)}, T_1^{(2)}, \dots, T_1^{(N_{\text{tot}})}$, for all the particles in the system. Normalized versions of the 1-body T matrices

and the irregular translation matrices^{1,4}, $H^{(j,k)}$, are then calculated via

$$\overline{T}_1^{(j)} \equiv [\xi^{(j)}] T_1^{(j)} [\psi^{(j)}]^{-1} \quad \overline{H}^{(j,k)} \equiv [\psi^{(j)}] H^{(j,k)} [\xi^{(k)}]^{-1} \quad (28)$$

where the diagonal matrices $[\psi^{(j)}]_{q,q',p,p'} = \delta_{q,q'} \delta_{p,p'} \psi_{n(p)}(kR_j)$ and $[\xi^{(j)}]_{q,q',p,p'} = \delta_{q,q'} \delta_{p,p'} \xi_{n(p)}(kR_j)$ respectively have Ricatti-Bessel and Ricatti-Hankel functions on the diagonal. (R_j being the radius of the circumscribing sphere of the j th scatterer).

The balanced recursive algorithm is that the solution for the $T_N^{(N,N)}$ matrix is obtained from the T matrices of the $N - 1$ system, $T_{N-1}^{(j,k)}$, via the matrix inversion in eq.(20). All the other matrices $\overline{T}_N^{(j,k)}$ with $j \neq N$ or $k \neq N$ are then obtained via matrix multiplications and additions via equations (22) and (24). This process is then repeated as many times as desired.

B. Physical quantities

When the incident field is a plane wave, it is convenient to express physical quantities in terms of cross sections. Appealing to the far-field approximation of the field, the extinction and scattering cross sections of clusters of N objects can be respectively expressed^{8,9}

$$\sigma_{\text{ext}} = -\frac{1}{k^2} \text{Re} \left[\sum_{k=1}^N a^{(j),\dagger} f_N^{(j)} \right] \quad \text{and} \quad \sigma_{\text{scat}} = \frac{1}{k^2} \sum_{j,k=1}^N f_N^{(j),\dagger} J^{(j,k)} f_N^{(k)} \quad (29)$$

It is also possible to produce analytical expression for local field quantities like individual absorption cross sections. For lossy scatterers in a lossless host medium, one can obtain individual particle absorption cross sections by integrating the Poynting vector on a circumscribing sphere surrounding the particle to obtain the formula as

$$\sigma_a^{(j)} = -\frac{1}{k^2} \text{Re} \left\{ f_N^{(j),\dagger} e_N^{(j)} \right\} - \frac{1}{k^2} \left| f_N^{(j)} \right|^2 \quad (30)$$

In an analogous fashion, optical forces on the particles can be calculated by integrating the Maxwell tensor on a circumscribing sphere surrounding the particle^{10,11}. It is frequently convenient to characterize the optical force by vector ‘cross sections’, $\vec{\sigma}_{\text{opt}}$, defined such that the time averaged optical force on particles immersed in a liquid dielectric of refraction index n_{med} can be expressed as

$$\mathbf{F}_{\text{opt}} = \|\mathbf{S}_{\text{inc}}\| \frac{n_{\text{med}}}{c} \vec{\sigma}_{\text{opt}} \quad (31)$$

where $\|\mathbf{S}_{\text{inc}}\| = \left\| \frac{1}{2} \text{Re}\{\mathbf{E}_{\text{inc}}^* \times \mathbf{H}_{\text{inc}}\} \right\|$ is the incident irradiance. The binding force and its associated cross section, σ_{b} , between two particles separated by a relative position vector $\mathbf{r}_{\text{pos}} \equiv \mathbf{r}_2 - \mathbf{r}_1$, can be defined as

$$F_{\text{b}} \equiv \frac{1}{2} (\mathbf{F}_2 - \mathbf{F}_1) \cdot \hat{\mathbf{r}}_{\text{pos}} \equiv \|\mathbf{S}_{\text{inc}}\| \frac{n_{\text{med}}}{c} \sigma_{\text{b}} \quad (32)$$

C. Interacting localized plasmon excitations

For those conductors, such as the noble metals, that support surface plasmon resonances, one can usually observe localized plasmon resonances in sufficiently small particles. These resonances are typically dominated by absorption if the particles are sufficiently small with respect to the incident wavelength and by scattering for larger particles. We chose to study silver spheres 50 nm in diameter immersed in air (for which both scattering and absorption are non-negligible).

The study is carried out for wavelengths ranging from the near ultra-violet through the visible (300 to 850 nm). We ignore the relatively modest finite size corrections to damping¹² and simply adopt the bulk dielectric constant of silver from ref.¹³ and extrapolate between the experimental values. The extinction, scattering and absorption cross sections for these particles are readily obtained from Mie theory and are displayed in figure 3 as a function of frequency. These spheres are quite small with respect to visible wavelengths, (size parameters in the 300↔800 nm wavelength range go through $kR = 0.52 \leftrightarrow 0.20$) and the isolated particle cross sections are obtained to high precision with $n_{\text{max}} = 4$. One can also see from figure 3 that the strength of the plasmon resonance for these particles is about half due to absorption and about half due to scattering.

One of the principal sources of interest of the localized plasmon resonances is their capacity to produce large field enhancements in regions much smaller than the incident field wavelength. This property is demonstrated in fig.4a) with a 2D and 1D plot of the electric field intensity in and near an isolated 50 nm diameter silver sphere illuminated near its resonance peak ($\lambda_0 = 365$ nm with $N_{\text{Ag}} = 0.077 + 1.6i$). The plots in Fig.4 are performed in a plane containing the center of the sphere and perpendicular to \mathbf{k}_{inc} (the polarization lies along the horizontal axis). The dimensionless extinction and scattering ‘efficiencies’, $Q = \sigma/(\pi R^2)$, at this frequency are respectively $Q_{\text{ext}} = 14.48$ and $Q_{\text{scat}} = 6.76$.

We now use the balanced recursive technique to calculate the optical response of a dimer composed of 50 nm diameter silver spheres whose surfaces are separated by 1 nm. Although

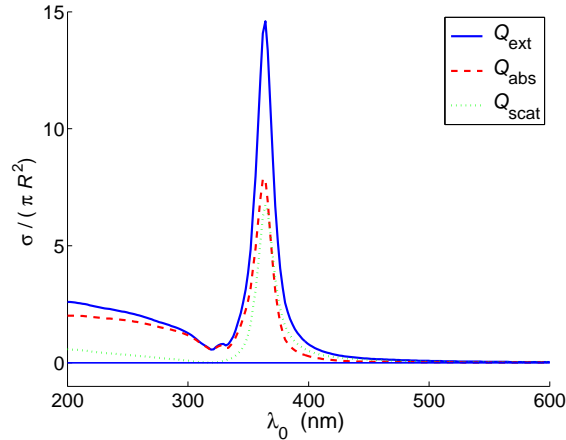


Fig. 3. Total cross section ‘efficiencies’, $Q \equiv \sigma/(\pi R^2)$ for an isolated 50 nm diameter sphere.

the T matrix calculated by RCTMA contains information for arbitrary incident fields, we study the physically interesting case of a plane wave perpendicular to the axis separating the particles. As is widely known, the response then depends strongly on the polarization of the incident light. In figures 5a) and 5c), the extinction and scattering cross sections per particle are presented when the polarization is respectively perpendicular and parallel to the symmetry axis. From figure 5c), one sees that the cross section for the parallel to axis polarization presents a two sphere coupled resonance that is strongly red-shifted with respect to the isolated particle resonance. The polarization perpendicular to this axis on the other hand presents only slight modifications with respect to an isolated sphere.

The optical binding force cross sections for these same polarizations are respectively plotted in figures 5b) and 5d). While the binding force for the polarization perpendicular to the particle axis (cf.5c)) is slightly repulsive, the force for polarization parallel to the resonance can be highly attractive with the dimensionless $|Q_b|$ attaining amplitudes of three orders of magnitude. There has already been experimental and theoretical evidence supporting the existence of optical force couplings in particles with plasmon excitations¹⁴ although such high precision calculations at such small separations seems not to have been presented before now.

This dimer system dramatically illustrates the ‘strong’ coupling category since correct calculations require that the VSWF space be enlarged far beyond the predominantly dipolar response characterizing the particles in isolation. The normalized cross sections per particle are given in the table 1 for different values of the VSWF space truncation. Although it was

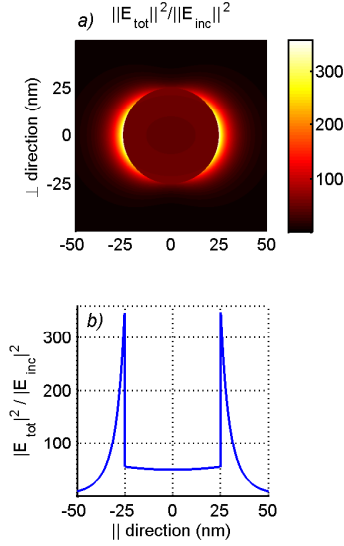


Fig. 4. Electric field intensity $\|\mathbf{E}_t\|^2/\|\mathbf{E}_{\text{inc}}\|^2$ in an isolated 50 nm diameter sphere ($\lambda_0 = 365$ nm, $N_{\text{Ag}} = 0.077 + 1.6i$). In a) is presented a 2D (hot) plot of the electric field intensity in a plane perpendicular to the wavevector and containing the origin of the sphere (the horizontal axis lies along the polarization direction). Fig b) is a 1D plot of the field intensity along the line in this plane containing the direction of electric field polarization.

necessary to go to $\sim n_{\text{max}} = 30$ to achieve 4 digit precision in all the cross sections, the table indicates that results were already quite good at $n_{\text{max}} = 20$.

A base 10 logarithmic intensity field map for a two silver sphere dimer illuminated with light polarized along the symmetry axis (frequency near the coupled sphere resonance maximum ($\lambda_0 = 467$ nm and $N_{\text{Ag}} = 0.048 + 2.827i$) is presented in figs.6a) and figs.6b) which are respectively a 2D plot (in the same plane as figure 4) and a 1D plot along the symmetry axis. The size parameter of the individual spheres is $kR = 0.34$ and the isolated cross sections at this frequency are $Q_{\text{ext}} = 0.136$ and $Q_{\text{scat}} = 0.0963$. As can be seen in fig.6, the fact that one had to go so far beyond the dipolar response has a dramatic effect on the field inside and near the the particles. Notably, the fields inside the particles are no longer quasi-constant as was the case for isolated particles.

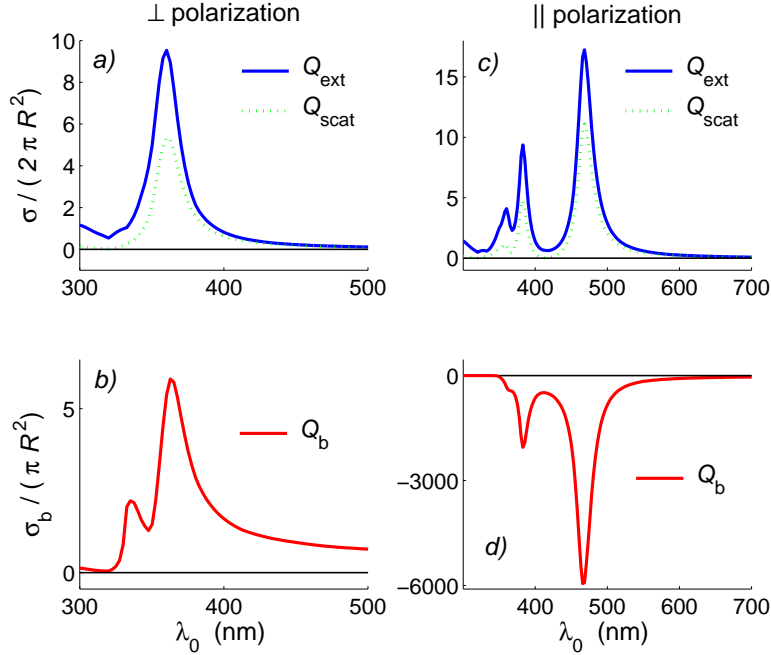


Fig. 5. Dimensionless cross section ‘efficiencies’ per particle, $Q = \sigma/(2\pi R^2)$ and binding force ‘efficiencies’ for a dimer of 50 nm diameter spheres (1 nm separation). In a) and b) the polarization is perpendicular to the symmetry axis and in c) and d) it is parallel to the symmetry axis.

n_{\max}	5	10	15	20	25	30	35	40
$Q_{\text{ext}}/2$	4.60	15.53	17.38	17.20	17.14	17.13	17.13	17.13
$Q_{\text{scat}}/2$	3.51	10.62	11.30	11.04	10.98	10.97	10.97	10.97
Q_b	-417	-3639	-5530	-5918	-6000	-6015	-6018	-6018

Table 1. Dimensionless cross section ‘efficiencies’ per particle in function of the VSWF truncation, n_{\max} . $Q_{\text{ext}} = \sigma_{\text{ext}}/(2\pi R^2)$, $Q_{\text{scat}} = \sigma_{\text{scat}}/(2\pi R^2)$ and $Q_b = \sigma_b/(\pi R^2)$. The system is a dimer composed of $D = 50$ nm diameter silver spheres (1 nm separation) at ($\lambda_0 = 467$ nm and $N_{\text{Ag}} = 0.048 + 2.827i$)

An important word of caution should be made at this point. Although 1 nm separation may appear to ‘nearly’ touching, the coupled resonance is in fact quite sensitive to exact separation details when resonant particles are so closely separated. For example, at a separation distance of 0.5 nm for the silver dimer, the coupled plasmon resonance is displaced to $\lambda_0 \simeq 516$ nm as compared with $\lambda_0 \simeq 467$ nm for a 1 nm separation, and the multipole order has to be pushed to $n_{\max} \simeq 50$ to achieve four digit accuracy in the cross sections. Nanometer scale separations are not necessarily theoretical idealizations however as recent

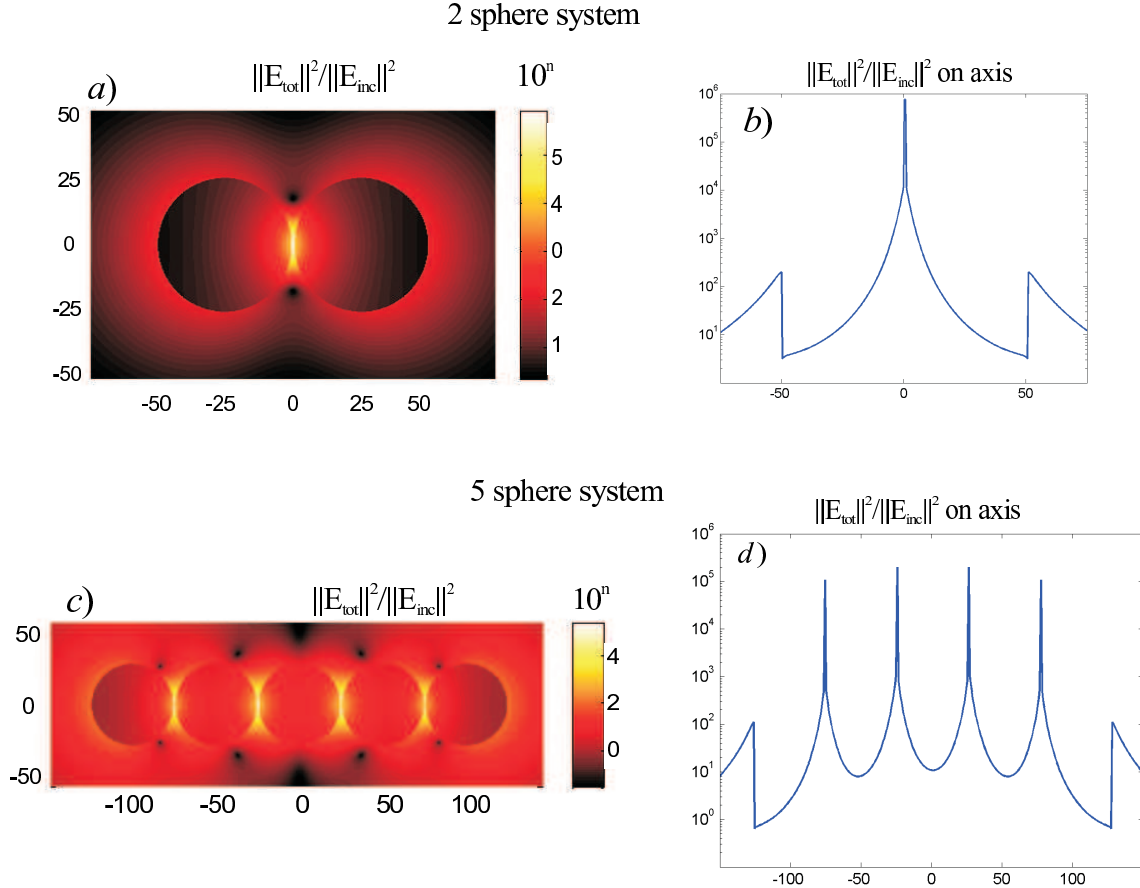


Fig. 6. Logarithmic scale plots of the field intensity for a two sphere dimer with ($\lambda_0 = 467$ nm and incident light polarized along the sphere axis ($N_{\text{Ag}} = 0.048 + 2.827i$)). In a) is a 2D plot in the plane containing the centers of the spheres and the polarization vector while b) is a 1D Logarithmic plot along the symmetry axis of the spheres. Figures. c) and d) are the same as a) and b) respectively but for a 5 sphere chain of spheres at its resonance maximum ($\lambda_0 = 561$ nm and $N_{\text{Ag}} = 0.0564 + 3.685i$). (cf. figure 7).

experiments with DNA separators have demonstrated¹⁵. Nevertheless, in applications like DNA separators, one may well have to consider the strong optical forces between these particles on account of the exceptionally strong attractive optical forces efficiencies of these resonances. For instance, the binding force efficiency at 0.5 μm separation was calculated at $Q_b = -20174$ for $\lambda_0 \simeq 515.6$ nm (cf. $Q_b = -6018$ for 1 nm separation at $\lambda_0 \simeq 467$ nm). The question of perfect spheres exactly in contact however seems untenable from an experimental standpoint and quite difficult from a theoretical standpoint on account of the singular behavior of the contact point. Theoretical ‘separations’ of 1\AA for instance require multipole truncations of the order of $n_{\text{max}} \gtrsim 120$ before convergence is achieved, but the idea of ‘perfect’ spheres separated by atomic scales has clearly gone beyond domain of applicability of our mesoscopic physical model in any case.

It is also important to verify that the recursive algorithm works for more complicated systems. Towards this end, we illustrate in figure 7, the results of calculations for a system composed a line of 5 identical silver spheres separated by 1 nm. For the binding force, we now present $Q_{b,1}$ which is the binding optical force between outermost spheres and their nearest neighbor and $Q_{b,2}$ which is the binding force between central sphere and each of its nearest neighbors. It is interesting to remark that addition of other spheres in the chain dramatically lessens the strong binding force interactions between spheres even though the fields between the spheres (cf. fig.5) can still be almost as high as the dimer case.

We remark that the interactions have continued to red-shift and widen the coupled “chain” resonance. This chain resonance peaks at ≈ 561 nm and $N_{\text{Ag}} \simeq 0.0564 + 3.685i$ ($Q_{\text{ext}}/5 = 14.416$ and $Q_{\text{scat}}/5 = 12.543$). It is clear from figure 7c) that the extinction cross section of the chain resonance is increasingly dominated by scattering rather than absorption. The number of VSWF orders necessary for high precision was also seen to decrease slightly for the chain. The calculation of fig.7 was carried out with $n_{\text{max}} = 20$ since calculations at $n_{\text{max}} = 24$ produced negligible differences on this scale.

Despite the dominance of scattering, a considerable amount of absorption is still present in the 5 sphere chain. Furthermore, from the field maps in figures 6c) and 6d), one can see that the central sphere has the highest field internal field intensities, and one consequently expects increased absorption in the central sphere. This supposition can readily be confirmed quantitatively by using eq.(30) to calculate the absorption in each individual sphere. The

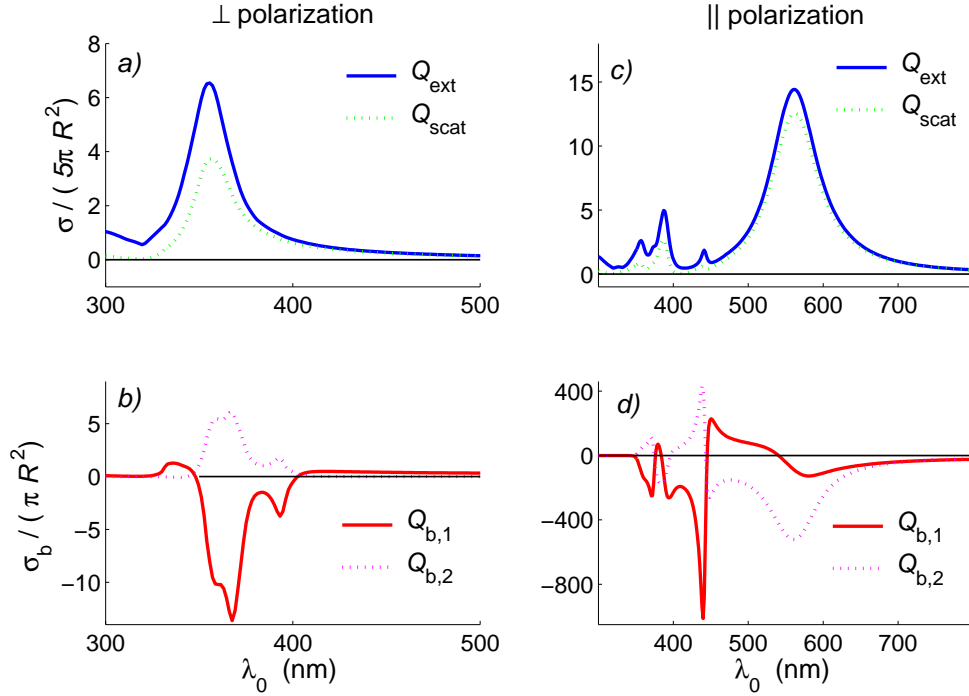


Fig. 7. Total cross section and binding ‘efficiencies’ for a line of 5 ‘touching’ silver spheres 50 nm in diameter (1 nm separation). In a) and b) the polarization is perpendicular to the symmetry axis and in c) and d) it is parallel to the symmetry axis.

results are given in table 2.

$Q_{a,1}$	$Q_{a,2}$	$Q_{a,3}$	$Q_{a,4}$	$Q_{a,5}$
0.8346	2.333	3.030	2.333	0.8346

Table 2. Individual absorption efficiencies $Q_{a,j} \equiv \sigma_{a,j}/(\pi R^2)$ in a five sphere chain at $\lambda_0 = 561$ nm and $N_{Ag} = 0.0564 + 3.685i$

We conclude this section with some calculations systems concerning larger chains of particles. One can remark that the chain coupled resonance continued to red-shift and widen when passing from the dimer to the five particle chain. Results for the extinction and scattering cross sections chains of 10 and 20 sphere chains are presented in figure 8 for the same polarizations and incident directions as considered previously.

One readily sees that ultraviolet and perpendicular responses per particle seem to have stabilized for large chains. The collective chain response on the other hand continued to

broaden and slightly red shift as one passed from 10 to 20 sphere chains and it is an interesting point for future studies to examine the evolution of this phenomenon for even longer chains and to study the impact of defaults in the chains.

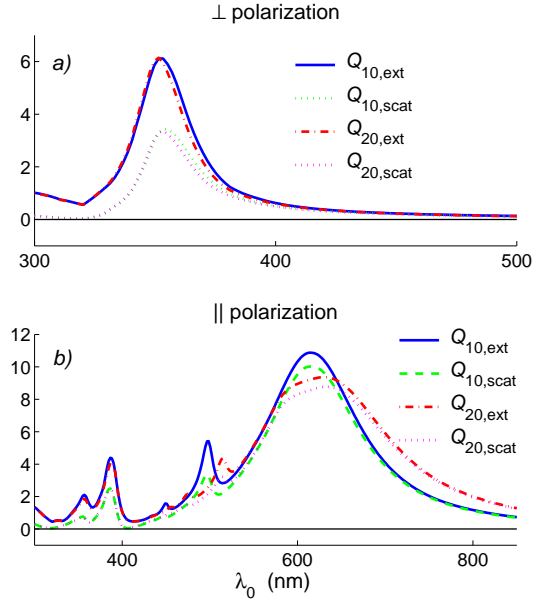


Fig. 8. Total extinction and scattering cross section efficiencies per particle in chains of 10 and 20 particles. In a) the polarization is perpendicular to the symmetry axis and in b) it is parallel to the symmetry axis.

6. Conclusions

The balanced recursive algorithm can give useful and highly accurate information in systems with large numbers of strongly interacting resonances. This has been demonstrated herein for the case of localized plasmon resonances and the studies presented here suggest that chains of closely spaced localized plasmons can have potentially interesting applications with respect to frequency shifting and broadening. Although not demonstrated here, this technique also proves useful for treating closely spaced systems possessing surface resonances of ‘whispering gallery’ type.

It is worth remarking that matrix balancing seems to be a useful method to employ in almost any Foldy-Lax equation solution scheme, be that for direct system matrix inversion, iterative techniques or linear system solutions. In fact, some modern matrix inversion programs actually integrate numerical matrix balancing into their algorithms. Nevertheless, since the matrix balancing in Foldy-Lax equations can be obtained analytically at relatively

low computational cost, it seems beneficial to carry out this balancing explicitly rather than relying on purely numerical treatments.

The matrix balanced RCTMA has potentially interesting applications for other kinds of resonance phenomenon, notably whispering Gallery modes. Such studies are currently underway. Furthermore, the ability of the matrix balanced RCTMA to study defaults and small modifications in large complicated systems is particularly promising and will be employed in subsequent studies.

Brian Stout and Alexis Devilez would like to thank Ross McPhedran, Evgeny Popov and Nicolas Bonod for helpful discussions. This work was funded in part by the grant ANR-07-PNANO-006-03 ANTARES of the French National Research Agency.

Appendix A: Vector spherical wave functions

The vector spherical wave functions can be readily written in terms of the Vector spherical harmonics (VSHs) and outgoing spherical *Hankel* functions :

$$\begin{aligned}\Psi_{1,p}(k\mathbf{r}) &\equiv \mathbf{M}_{nm}(k\mathbf{r}) \equiv h_n^+(kr) \mathbf{X}_{nm}(\theta, \phi) \\ \Psi_{2,p}(k\mathbf{r}) &\equiv \mathbf{N}_{nm}(k\mathbf{r}) \equiv \frac{1}{kr} \left[\sqrt{n(n+1)} h_n^+(kr) \mathbf{Y}_{nm}(\theta, \phi) + [kr h_n^+(kr)]' \mathbf{Z}_{nm}(\theta, \phi) \right] \quad (\text{A1})\end{aligned}$$

In the same manner, the regular VSWFs are obtained by replacing the spherical Hankel functions in eq.(A1) by spherical *Bessel* functions. Our adopted definition of the VSHs is

$$\mathbf{Y}_{nm}(\theta, \phi) \equiv \hat{\mathbf{r}} Y_{nm}(\theta, \phi) \quad \mathbf{Z}_{nm}(\theta, \phi) \equiv \frac{r \nabla Y_{nm}(\theta, \phi)}{\sqrt{n(n+1)}} \quad \mathbf{X}_{nm}(\theta, \phi) \equiv \mathbf{Z}_{nm}(\theta, \phi) \wedge \hat{\mathbf{r}} \quad (\text{A2})$$

where the $Y_{nm}(\theta, \phi)$ are the scalar spherical harmonics.

References

1. B. Stout, J.-C. Auger, and J. Lafait, “A transfer matrix approach to local field calculations in multiple scattering problems,” *J. Mod. Opt.* **49**, 2129–2152 (2002).
2. J.-C. Auger and B. Stout, “A recursive centered T-Matrix algorithm to solve the multiple scattering equation : numerical validation,” *J. Quant. Spect. & Rad. Trans.* **79-80**, 533–547 (2003).
3. A. Doicu and T. Wriedt, *Light Scattering by Systems of Particles* (Springer, 2006).
4. L. Tsang, J. A. Kong, and R. T. Shin, *Theory of Microwave Remote Sensing* (John Wiley & Sons, 1985).

5. W. C. Chew, *Waves and Fields in Inhomogeneous Media* (IEEE Press, New York, 1994).
6. M. Lax, "Multiple Scattering of Waves," *Rev. Mod. Phys.* **23**, 287–310 (1951).
7. B. Stout, C. Andraud, S. Stout, and J. Lafait, "Absorption in multiple scattering systems of coated spheres," *J. Opt. Soc. Am. A* **20**, 1050–1059 (2003).
8. B. Stout, J.-C. Auger, and J. Lafait, "Individual and aggregate scattering matrices and cross sections : conservation laws and reciprocity," *J. Mod. Opt.* **48**, 2105–2128 (2001).
9. D. W. Mackowski, "Calculation of total cross sections in multiple-sphere clusters," *J. Opt. Soc. Am. A* **11**, 2851–2861 (1994).
10. O. Moine and B. Stout, "Optical force calculations in arbitrary beams by use of the vector addition theorem," *J. Opt. Soc. Am. B* **22**, 1620–1631 (2005).
11. M. I. Mishchenko, L. D. Travis, and A. Lacis, *Scattering, Absorption and Emission of Light by Small Particles* (Cambridge University Press, 2002).
12. C. F. Bohren and D. R. Huffman, *Absorption and Scattering of Light by Small Particles* (Wiley-Interscience, New York, 1983).
13. E. . D. E. Gray, *American Institute of Physics Handbook 3rd edition* (Mcgraw-Hill Tx, 1972).
14. Z. Li, M. K all, and H. Xu, "Optical forces on interacting plasmonic nanoparticles in a focused Gaussian beam," *Phys. Rev. B* **77**, 085,412 (2008).
15. S. Bidault, F. J. G. Abajo, and A. Polman, "Plasmon-Based Nanolenses Assembled on a Well-Defined DNA Template," *J. AM. Chem. S.* **130**, 2750-2751 (2008).